Article title:

Exergo-technological explicit methodology for gas-turbine system optimization for series hybrid electric vehicles

Author names and affiliations:

Wissam S Bou Nader[1,4], Charbel J Mansour[2], Maroun G Nemer[3] and Olivier M Guezet[4]

[1] Ecole des Mines de Paris, Centre Efficacité Energétique des Systèmes CES, Palaiseau, France wissam.bou_nader@mines-paristech.fr

[2] Industrial and Mechanical Engineering department, Lebanese American University, New York, United-States charbel.mansour@lau.edu.lb

[3] Centre Efficacité Energétique des Systèmes CES, Ecole des Mines de Paris, Palaiseau, France maroun.nemer@mines-paristech.fr

[4] PSA Group, Centre technique de Vélizy, Vélizy, France wissam.bounader@mpsa.com, olivier.guezet@mpsa.com

Corresponding author:

Wissam Bou Nader

Email: wissam.bounader@mpsa.com
PSA Group
Technical Center of Vélizy
Route de Gizy
78943 Vélizy Villacoublay Cedex
P.O Box VV1415

Email: wissam.bou_nader@mines-paristech.fr
Ecole des Mines de Paris,
Centre Efficacité Energétique des Systèmes CES,
5 rue Léon Blum
91120 Palaiseau, France

Acknowledgement:

-

Original Article

Exergo-technological explicit methodology for gas-turbine system optimization for series hybrid electric vehicles

Wissam S Bou Nader[1,4], Charbel J Mansour[2], Maroun G Nemer[3] and Olivier M Guezet[4]

[1] Ecole des Mines de Paris, Centre Efficacité Energétique des Systèmes CES, Palaiseau, France wissam.bou_nader@mines-paristech.fr

[2] Industrial and Mechanical Engineering department, Lebanese American University, New York, United-States charbel.mansour@lau.edu.lb

[3] Centre Efficacité Energétique des Systèmes CES, Ecole des Mines de Paris, Palaiseau, France maroun.nemer@mines-paristech.fr

[4] PSA Group, Centre technique de Vélizy, Vélizy, France wissam.bounader@mpsa.com, olivier.guezet@mpsa.com

Abstract

Significant research efforts have been invested in the automotive industry on hybrid-electrified powertrains in order to reduce the passenger cars' dependence on oil. Powertrains electrification resulted in a wide range of hybrid vehicle architectures. Fuel consumption of these powertrains strongly relies on the energy converter performance, as well as on the energy management strategy deployed on-board. This paper investigates the potential of fuel consumption savings of a series hybrid electric vehicle (SHEV) using a gas turbine (GT) as energy converter instead of the conventional internal combustion engine (ICE). An exergo-technological explicit analysis is conducted to identify the best GT-system configuration. An intercooled regenerative reheat cycle is prioritized, offering higher efficiency and power density compared to other investigated GT-systems. A SHEV model is developed and powertrain components are sized considering vehicle performance criteria. Energy consumption simulations are performed on the worldwide-harmonized light vehicles test procedure (WLTP) driving cycle using dynamic programing as global optimal energy management strategy. A sensitivity analysis is also carried out in order to evaluate the impact of the battery size on the fuel consumption, for self-sustaining and plug-in hybrid SHEV configurations. Results show 22% to 25% improved fuel consumption with GT as auxiliary power unit (APU) compared to ICE. Consequently, the studied GT-APU presents a potential for implementation on SHEVs.

Keywords

Gas turbine, exergy analysis, series hybrid, dynamic programming, global optimization.

1. Introduction

Different manufacturers have investigated the integration of gas turbines (GT) in conventional powertrains over years as the main energy converter instead of conventional internal combustion engines (ICE). Early GT vehicle models in the 60's and 70's showed poor acceleration response and higher fuel consumption compared to internal combustion engine vehicles (ICEV) [1, 2]. These drawbacks where mainly due to operating the GT at high speed even at idle conditions, in addition to mechanically coupling the turbine to the vehicle driving load, which resulted in a low efficiency operating range of the GT-system. Despite the many technological advancements and improvements made later on GTs such as variable turbine geometry, water injection for improving the performance, and increase of turbine inlet temperature (TIT), the acceleration lag and the poor fuel efficiency were still the main reasons hindering their deployment in conventional powertrains.

A review of recent research and development programs of automotive manufacturers revealed new interests in GT for automotive applications, demonstrated in several vehicle concept cars. Moreover, the review of the recent literature showed interesting insights on GT consumption and emissions reductions. A study on GT for automotive applications at Chalmers University of Technology, presented an interest in operating GT at optimal efficiency point compared to ICE [3]. A complementary study at the University of Rome showed that GT emissions at optimal efficiency operation meet the Euro 6 emissions levels of CO, NOx and soot even without the use of after-treatment systems [4]. In addition, GT-systems offer other intrinsic benefits for vehicle powertrains such the reduced number of moving parts, vibration-free operation, low maintenance cost, high durability and the absence of cooling system [1].

Based on the aforementioned findings, GT-systems present a forthcoming potential for improving modern vehicle efficiency and emissions, with the benefit of fuel-use flexibility when compared to ICEVs; particularly, in series hybrid electric vehicle technologies (SHEV). Series hybrid powertrains combine a thermal and an electric powertrain in a series energy-flow arrangement, as illustrated in figure 1. The thermal powertrain is constituted of an energy converter and an electric generator, and is referred to as Auxiliary Power Unit (APU). The APU is mainly used to recharge the battery once depleted, and the electric powertrain provides the necessary power to overcome the driving load. Consequently, the APU operating speed is cinematically decoupled from the vehicle velocity, and the energy converter operating point is easily controllable to meet its best efficiency.

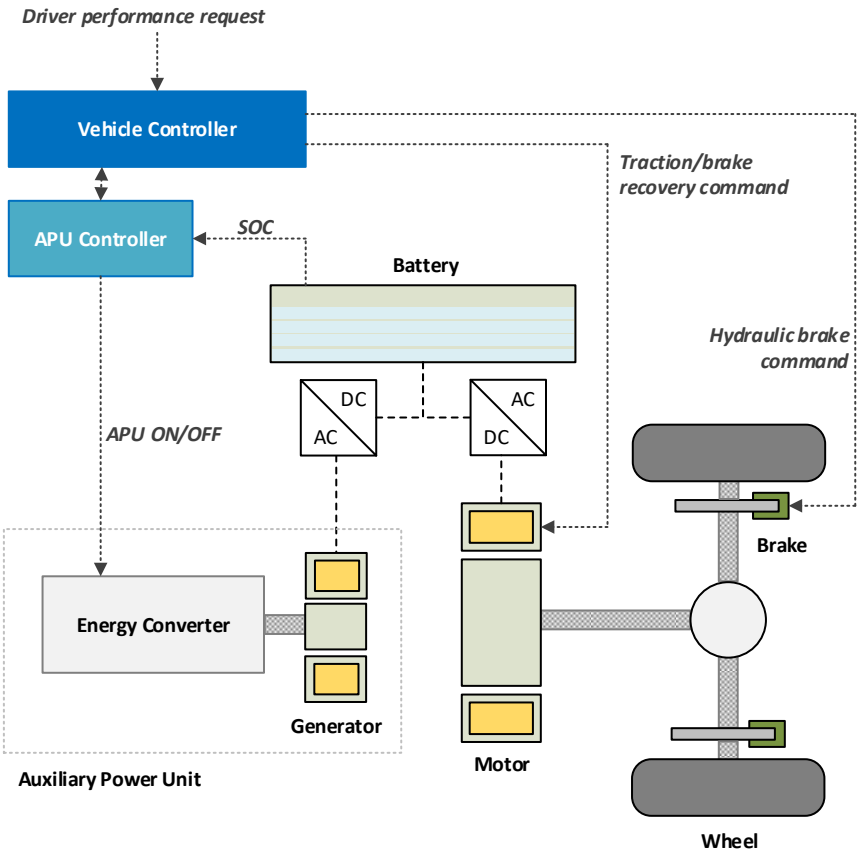

Figure 1: Powertrain configuration of series HEV.

On another hand, several GT-system options could be considered for integration in SHEVs, combining a basic GT to heat recovery systems and single or multi-stage compressions and expansions. There have been numerous studies published over the past decade in the academic literature covering a multitude of GT-system configurations and performance analysis in different applications, such as industrial [5-15] and aeronautics [16, 17]. The survey of these studies confirms

that most GT-systems are designed based on efficiency optimization, power density optimization or a compromise between the two criteria. For instance, industrial GT-system studies focused on finding an acceptable compromise between maximizing the system efficiency and the power density, with less concern on reducing the weight [7-13]. Along these lines, aeronautical GT-system studies focused on maximizing the power density due to the high weight-reduction priority constraint for such applications [17]. In both applications, a combination of several measures was required such as the need to increase TIT, to add intercooler, regenerator and reheat systems in order to achieve the needed optimization [9, 16, 17]. However, there have only been a few recent papers on GT-systems suitable for automotive applications [18-20] due to the lack of competitiveness of GT compared to ICE in conventional powertrains. Other papers date for more than 20 years [21-24]. The review of these recent and old studies underlines the following two gaps:

- No specific methodology on selecting the best-suited GT-system for automotive applications is adopted. The studies focus is on the performance investigations of some pre-defined GT-systems, without taking into consideration any optimization requirement or technological constraints.
- The overall vehicle consumption under driving conditions is not evaluated and benchmarked against ICEV. These studies did not provide a complete vehicle model integrating the investigated GT-systems into a powertrain model, supervised by an energy management strategy.

Therefore, based on the above synthesis of the insights and gaps in the literature for re-adopting GT in automotive applications, this study proposes a comprehensive methodology to identify the potential GT-system options and select the optimal system configuration for SHEV application. A methodology for identification and assessment of the different GT-system options applicable to SHEV are carried out in section 2, based on exergy analysis and automotive technological constraints. Observed results are then used for the prioritization and the selection of the optimal GT-system configuration. The selection criterion is optimizing the system efficiency. Thereafter, the identified GT-system is integrated in an SHEV model in section 3, and a comparison between two SHEV models with different APU technologies (GT-APU and ICE-APU) is presented. SHEV models are developed with a backward-modeling approach, and the powertrain components are sized according to automotive performance criteria such as the maximum vehicle speed and acceleration. Finally, energy consumption simulations of both models are compared on the WLTP driving cycle, and a sensitivity analysis illustrating the battery size impact on energy consumption is presented. Note that Dynamic Programing (DP) is adopted as Energy Management Strategy (EMS) in order to provide the global optimal strategy to power ON and OFF the APU. Consequently, the analysis considers only the impact of the GT-system on consumption and excludes the influence of rule-based EMS [25, 26].

This study is novel in three ways: first, it is the first study to consider an exergo-technological explicit analysis for the prioritization and identification of the most efficient GT-system to be deployed in an SHEV among a variety of possible GT-system options. Second, it presents a comprehensive methodology for modeling, component sizing and fuel consumption assessment of a serial hybrid powertrain using GT-system as APU energy converter and dynamic programming for global optimal energy management strategy. Third, the study provides a comparative consumption assessment, between SHEVs of similar performance with GT-APU and ICE-APU.

2. Methodology for Optimal Gas Turbine System Selection

This section presents the methodology adopted to evaluate the potential of GT-systems in SHEVs. It consists of two-steps assessment plan, as described in sections 2.1 and 2.2, and summarized in figure 2. The first assessment step consists of an energy and exergy analysis applied to the basic GT cycle,

where the system efficiency, specific work, and exergy are calculated. Based on the resulting exergy destructions in the system, modifications of the basic GT cycle are presented, by considering several measures such as heat recovery and multi-stage compressions among others, in order to reduce exergy losses. Accordingly, the list of potential GT-system configurations is identified.

The energy and exergy calculations are then carried out in the second assessment step on all identified configurations. Components technological constraints and automotive design constraints are considered, and the optimal-realistic GT-system configuration for the SHEV application is selected. Components technological constraints such as the maximum TIT, the maximum compression ratio per stage and the maximum components' efficiencies are based on state-of-the-art data of available and newly developed technologies for automotive applications. However, automotive design constraints such as the number of compression and expansion stages, the power density and the number of heat exchangers are applied in order to simplify the system-integration complexity in vehicles.

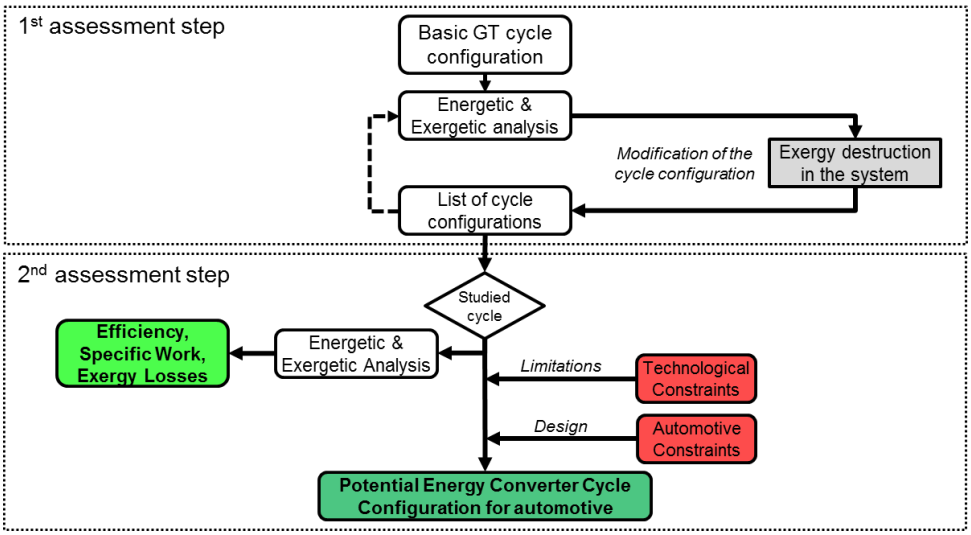

Fig. 2. Exergo-technological explicit selection method of the best-suited GT-system for SHEV application.

2.1. Energy and exergy analysis of simple gas-turbine system

In this section, the modeling of the basic Brayton GT cycle, which consists of a compressor, a combustion chamber and a turbine, is presented. First law of thermodynamics is applied to each component in order to deduce the cycle thermal efficiency and power density. Exergy analysis is then carried out in order to trace the work losses in the system, their types and quantities, in order to better inform on the possible options to reduce the inefficiencies. Energy and exergy model equations for each component are available in thermodynamic fundamentals books such as [27-28]. Note that the exergy destruction calculations for the combustion chamber presented in the literature requires the use of Gibbs function value for fuel; however, it was substituted in this study by equation (1), where the average temperature in the combustion chamber is estimated from (2) [29-31].

$$e_{d\_CC} = \frac{T_0}{\check{T}} . \Delta Q_{CC} \tag{1}$$

$$\check{T} = \frac{\Delta Q_{CC}}{\Delta S_{CC}} = \frac{h_{CC,outlet} - h_{CC,inlet}}{S_{CC,outlet} - S_{CC,intlet}} \tag{2}$$

With e_{d_CC} : Exergy destruction in the combustion chamber (kJ/kg)

$\check{T}$: Average temperature in the combustion chamber (K)

ΔQ_{CC} : Enthalpy difference in the combustion chamber (kJ/kg)
ΔS_{CC} : Entropy difference in the combustion chamber (kJ/kg.K)
T_0 : Reference temperature (K)

Exergy destruction results of the investigated basic GT-system are illustrated in figure 3. The figure points out the two highest shares of exergy losses, occurring in the combustion chamber and the exhaust gas at the turbine outlet.

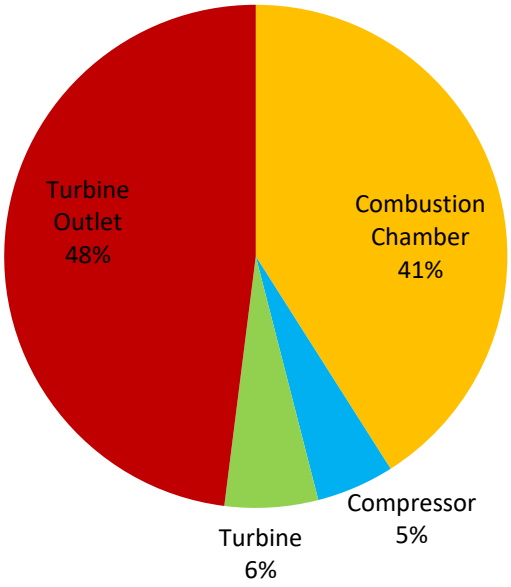

Fig. 3. Distribution of exergy destruction in the Brayton gas-turbine system with turbine inlet temperature of 1250°C and maximum cycle pressure of 1.2 MPa.

It was demonstrated in several studies [30-32] that the exergy destruction in the combustion chamber decreases as the average temperature increases. Accordingly, two ways can be considered to decrease these exergy losses: (1) increasing the TIT while respecting metallurgic constraints, and (2) increasing the average combustion temperature through a regenerator upstream of the combustion chamber.

As for the second major source of exergy destruction, losses from the exhaust gases at the turbine outlet to the ambient air can be recovered by adopting waste heat recovery systems. Two recovery options are applicable: (1) an external heat recovery system through a steam Rankine bottoming cycle, and (2) an internal heat recovery system, using a regenerator.

The exergy destruction shares of the compressor and turbine illustrated in figure 3 can be reduced by improving the efficiency of these components.

Based on these findings, the list of the different GT-system options considered in this study is presented below, based on the combination of the suggested techniques for exergy losses reduction as illustrated in figure 4. The considered GT-system options are as follow:

1. Combined Cycle Gas Turbine, with GT coupled to a steam Rankine cycle (CCGT)
2. Regenerative GT (RGT)
3. Regenerative GT with Organic Rankine Cycle (RGT-ORC, with 1234yf working fluid)
4. Intercooled Regenerative GT (IRGT)
5. Intercooled Regenerative Reheat GT (IRRGT)
6. Isothermal Compression Regenerative GT (ICRGT)
7. Isothermal Compression Regenerative Reheat GT (ICRRGT)

8. Isothermal Compression Regenerative Isothermal Expansion GT (ICRIEGT)

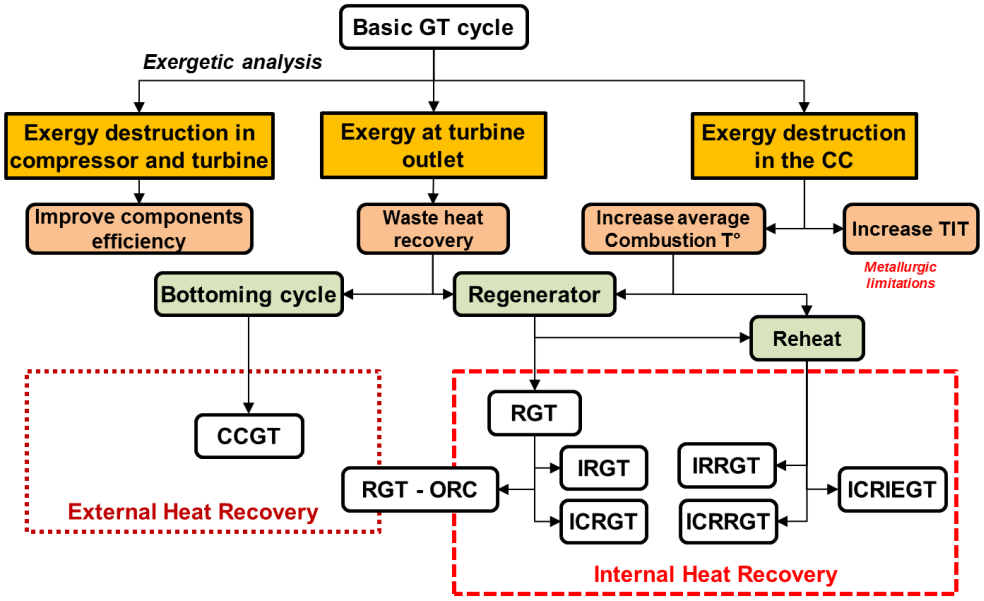

Fig. 4. Exergy assessment methodology for the identification of the GT-system options with reduced exergy losses in a basic GT-system.

Note that the efficiency and power density of the GT-system options 4 and 5 can be further improved if isothermal compression and expansion are considered. In fact, the isothermal compression maximizes the heat recovery process in the regenerator, and the isothermal expansion maximizes the expansion work [16, 32]. To this end, isothermal compressions are considered in ICRGT, ICRRGT and ICRIEGT and isothermal expansion in ICRIEGT (options 6 to 8). Although isothermal processes are technically difficult to achieve and remain currently theoretical, they are considered in this study for comparison purposes, and to emphasize their additional benefits. Nevertheless, many studies in the literature investigated technical options for getting close to isothermal processes such as reheat cycles [8], intercooling compression [17], isothermal combustion cycles [32] and cooling compression with water or liquid nitrogen [33].

Triple stage compressions were also considered in the analysis; however, results did not reflect substantial additional advantage compared to the dual stage compression. Therefore, due to the additional complexity in vehicle integration for little improvements, triple compression cycles were disregarded and only dual stage compressions are considered.

2.2. Energy and exergy analysis of identified potential gas-turbine systems

The identified GT-system options of figure 4 are assessed here in order to prioritize these options based on their respective efficiency and net specific work, and select the most suitable configuration. The assessment methodology for each option is illustrated in figure 5. Energy and exergy calculations are performed first with Refprop software, using the set of physical parameters such as the TIT, the cycle pressure, the components efficiencies, among others; as summarized in table 1. These parameters correspond to the state-of-the-art specifications and limitations of GT component technologies and to automotive design constraints.

The energy and exergy calculations are made as function of two parametric design criteria: the compression ratio (π_i) and the expansion ratio (β_j), with *i* and *j* referring to the number of compressors and turbines respectively. Therefore, the second calculation step uses the NSGA multi-objective

genetic algorithm to determine the Pareto optimal efficiency and net specific work solutions for the optimal (π_i) and (β_j) [34]. Figure 6 illustrates the resulting Pareto optimal solution curves for the different assessed GT-systems. For the rest of the study, the comparison between the different GT-systems will be based on the best efficiency points on the Pareto curves. Therefore, the selection of the best-suited GT-system for SHEV will be made with respect to the highest efficiency among the compared systems.

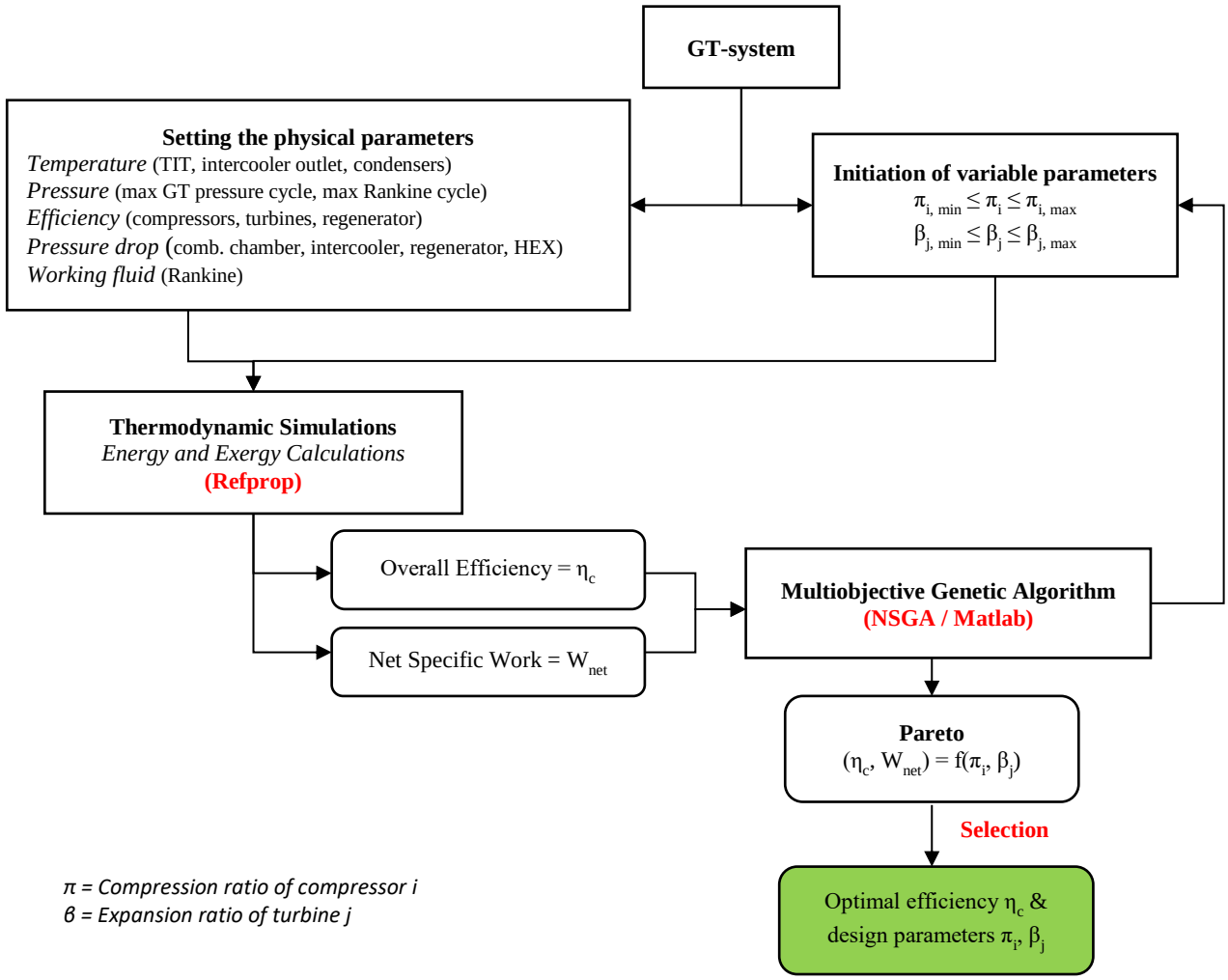

Fig. 5. Assessment methodology for the identification of the highest efficiency GT-system and its optimal design parameters.

Table 1. Simulation parameters based on state-of-the-art component specifications and automotive design constraints.

Parameter	Unit	Value	Parameter	Unit	Value
Compressor technology	-	Radial	Combustion chamber pressure drop	%	4
Max number of compression stages	-	2	Max number of expansion stages	-	2
Compressor maximum pressure ratio	-	4	Turbine Inlet Temperature (TIT)	°C	1250
Compressors efficiency	%	80	Turbines isentropic efficiency	%	85
Compressor inlet pressure drop	%	0.5	Turbine expansion ratio	-	3.5
Maximum cycle pressure	MPa	1.2	Steam Rankine max pressure	MPa	8
Intercoolers pressure drop	%	5	Steam condensing temperature	°C	100
Intercoolers outlet temperature	°C	60	ORC/SRC pump and turbine eff.	%	80 and 85
Regenerator efficiency	%	85	ORC fluid	-	1234yf
Regenerator pressure drop cold side	%	4	Organic Rankine max pressure	MPa	3

Regenerator pressure drop hot side	%	3	Organic condensing temperature	°C	45

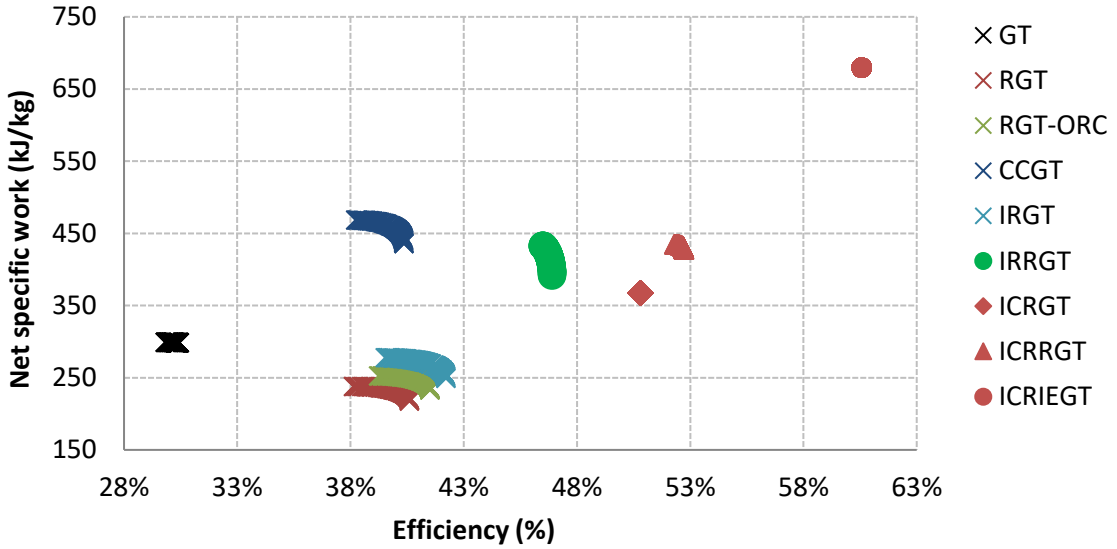

Fig. 6. Pareto optimal efficiency and net specific work solutions of the different GT-systems.

Figures 7 and 8 illustrate the efficiency, net specific work and optimal compression and expansion ratio simulation results of the investigated GT-systems, compared to the ICE. ICRIEGT presents the highest efficiency and net specific work; however, as discussed in the previous section, this cycle is not realistic for implementation in SHEV since it relies on isothermal compression and expansion. Consequently, IRRGT (figure 9) is the optimal-realistic GT-system considered for the rest of this study, which emulates the isothermal compression and expansion of ICRIEGT through a dual stage compression with an intercooler and a dual-expansion turbine with a reheat system.

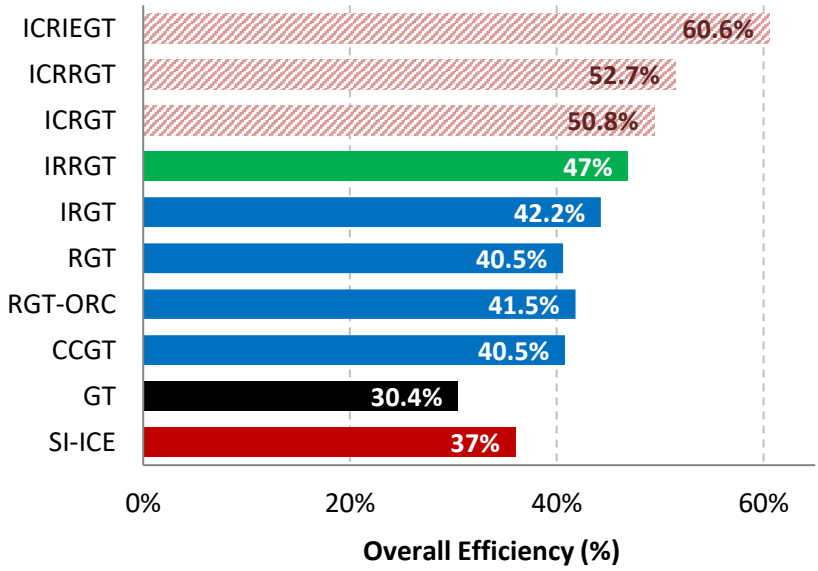

Fig. 7. Optimum efficiency comparison of ICE and the investigated GT-system options.

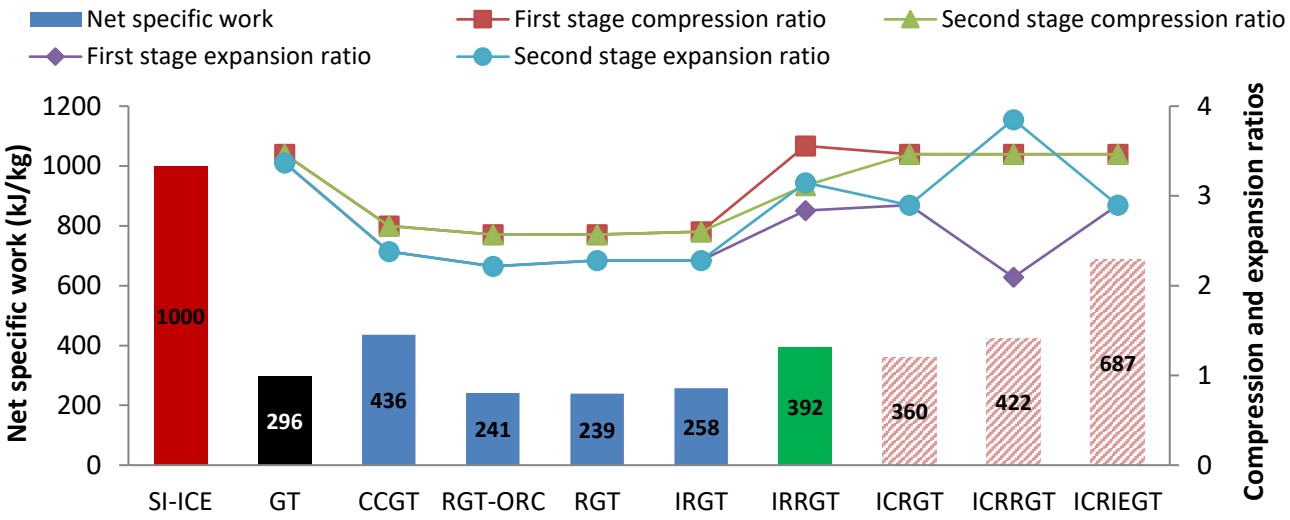

Fig. 8. Net specific work of ICE and the investigated GT-system options at optimal efficiency.

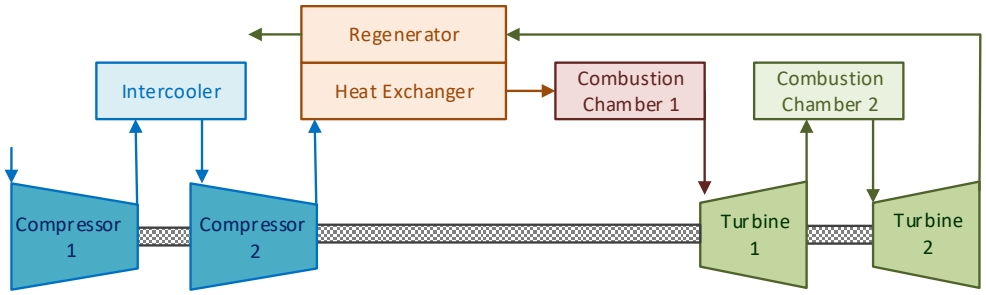

Fig. 9. Intercooled Regenerative Reheat Gas Turbine Cycle (IRRGT-system).

3. Vehicle Model

3.1. Powertrain setup and components sizing

In order to evaluate the benefits of the IRRGT-system in terms of fuel savings compared to ICE, a medium-class series hybrid vehicle, consisting of an IRRGT-APU and an electric traction system (as illustrated in figure 1) is modelled and presented in this section. Series configuration presents the advantage of tackling the two main deficiencies of GT-systems in automotive applications as discussed in the literature: the poor efficiency and the acceleration lag. On one side, the IRRGT operates in an SHEV at steady power corresponding to the optimum efficiency, which is higher than the maximum efficiency of ICE (as illustrated in figure 7). On the other side, the vehicle is propelled by an electric motor, powered by a battery and/or the APU, and properly sized to ensure the vehicle acceleration and velocity performance without deficiency.

The electric traction motor is sized in order to ensure similar performance to a medium class hybrid vehicle, with maximum speed of 160 km/h and acceleration from 0-100 km/h in 9.6 s, using equation (A.1) from appendix A. Around 80 kW tractive power is needed to accelerate the vehicle, compared to 40 kW to maintain it at 160 km/h. Consequently, the selected electric traction motor is 80 kW.

The APU is used to ensure the battery sustainability under all driving conditions. Hence, the IRRGT and the electric generator are sized taking into consideration urban stop-and-go patterns and highway-driving patterns. The urban stop-and-go patterns are represented in this study by the WLTP, and the

average load power is computed using equation (A.2). The highway-driving pattern is emulated as driving for a long distance at the maximum velocity of 160 km/h without the need of the battery support, using equation (A.3). 40 kW are required to propel the vehicle at maximum speed on highway compared to 10.4 kW for the WLTP urban-patterns. Hence, a 40 kW IRRGT is considered.

As for sizing the battery, power and capacity have to be considered. Under any driving conditions, the battery must provide sufficient traction power, with the support of the APU under extreme power demand. Consequently, battery maximum power is sized with respect to the electric motor maximum power and the APU power, using equation (A.4). A 50 kW battery is considered. As for the capacity, four different values of 2, 5, 10 and 20 kWh are considered in the analysis in order to assess the impact of the battery size on improving fuel consumption. The additional battery mass with the increased capacity is taken into account. Values were retrieved from commercialized battery specifications, as illustrated in figure 10.

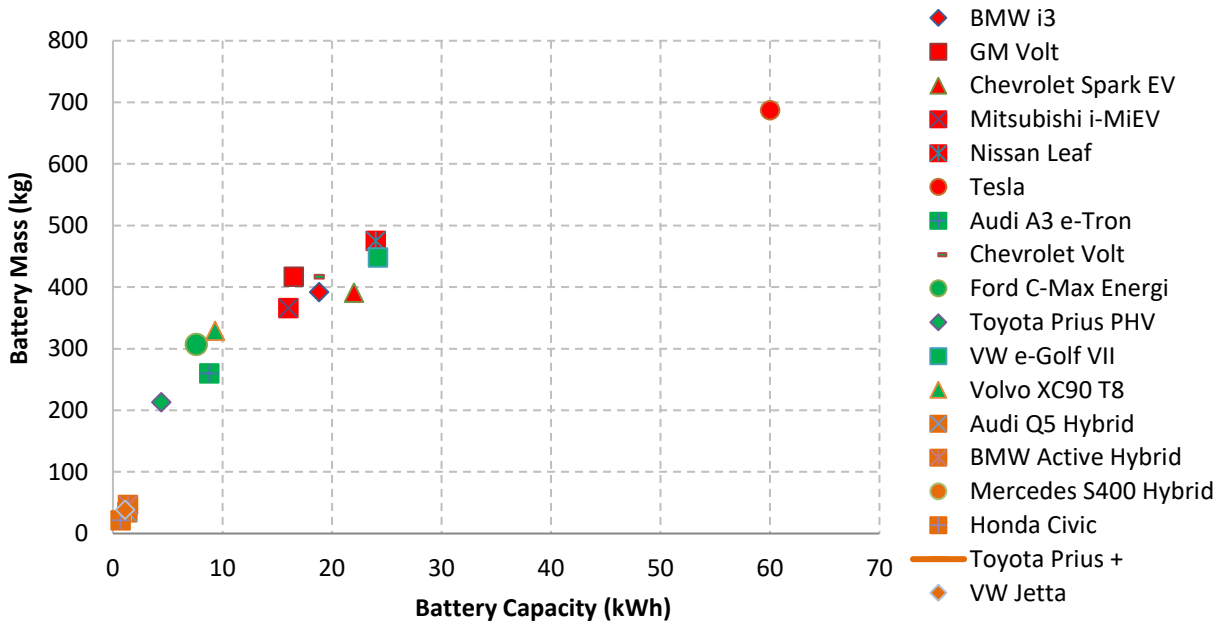

Fig. 10. Battery capacity as function of battery mass for the different commercialized HEV (in orange), PHEV (in green) and EV (in red).

Based on the above, table 2 summarizes the vehicle parameters needed for modeling the SHEV. Equations (3) to (10) present the powertrain backward model. Note that longitudinal dynamics of the chassis are only considered and on flat roads. It is also noteworthy to mention that the mass of the GT-system, the generator and the electric motor are considered equal to the mass of the engine and its accessories. In fact, it was presented in [18, 23] that the power density of a 75kW GT-system combined to a generator and a 90 kW electric motor is in the range of 375 W/kg, slightly better than the 350 W/kg of the considered ICE in this study.

Table 2: Vehicle and components specifications.

Vehicle specifications	**Symbol**	**Unit**	**Value**
Vehicle mass (including driver)	M_v	kg	1210
Frontal area	S	m^2	2.17
Drag coefficient	C_x	-	0.29
Wheel friction coefficient	f_r	-	0.0106
Air density	ρ	kg/m3	1.205
Wheel radius	R_w	m	0.307
Auxiliaries consumption	P_{aux}	W	750
Battery maximum power	$P_{b\ max}$	kW	50

Battery capacity	C_b	kWh	2, 5, 10, 20
Battery mass	M_b	kg	86, 188, 259, 356
Battery state of charge	SOC	-	[0.2, 0.4, 0.6, 0.8, 1]
Battery open circuit voltage	V_{oc}	V	[220, 224, 227, 228, 251]
Battery internal resistance	R_i	Ohm	[0.315, 0.31, 0.31, 0.335, 0.385]
IRRGT-system power	P_{GT}	kW	40
IRRGT efficiency	η_{GT}	%	46.9
Generator maximum power	P_g	kW	45
Generator maximum efficiency	η_g	%	95
Motor maximum power	P_m	kW	80
Motor maximum efficiency(1)	η_m	%	93
Transmission ratio	i	-	5.4
Transmission efficiency	η_t	%	97
Vehicle total mass	M_t	kg	$M_v + M_b$
Fuel heating value	H_v	MJ/kg	44.8
(1) The model includes a torque-speed efficiency map of the electric motor.			

$$P_{load}(t) = \left(\frac{1}{2}\rho S C_x v(t)^2 + M_t g f_r\big(v(t)\big) + M_t \frac{dv(t)}{dt}\right) \times v(t) \tag{3}$$

$$P_m(t) = \begin{cases} \dfrac{P_{load}(t)}{\eta_t \times \eta_m}, & \dfrac{dv}{dt} \geq 0 \\ P_{load}(t) \times \eta_t \times \eta_m, & \dfrac{dv}{dt} < 0 \end{cases} \tag{4}$$

$$P_g(t) = u(t) \times P_{GT} \times \eta_g \tag{5}$$

$$P_{total}(t) = P_m(t) + P_{aux}(t) \tag{6}$$

$$P_b(t) = P_{total}(t) - P_g(t) \tag{7}$$

$$I_b(t) = \frac{V_{oc}\big(SOC(t)\big) - \sqrt{V_{oc}^2\big(SOC(t)\big) - 4P_b(t)R_i\big(SOC(t)\big)}}{2R_i\big(SOC(t)\big)} \tag{8}$$

$$SOC(t) = SOC_i(t) + \frac{1}{C_b}\int_{t_0}^{t} I_b(t)dt \tag{9}$$

$$\dot{m}_f(t) = \begin{cases} \dfrac{P_{GT}(t)}{\eta_{GT} \times H_v}, & APU{:}\,ON \\ 0, & APU{:}\,OFF \end{cases} \tag{10}$$

3.2. Energy Management Strategy

Two distinct controllers are considered in the model as illustrated in figure 1: the vehicle controller and the APU controller. The vehicle controller is in charge of meeting the driver request in terms of performance. Hence, its main objective is to control the electric motor power in order to meet the traction and brake energy recovery demand, as presented in equation (4). The APU controller monitors the battery SOC; thus, it controls the APU operations in order to maintain the SOC in the desired range. Therefore, an engine on/off variable $u(t)$ is considered in equation (5) in order to control the APU start operations. $u(t)$ takes the value of 0 for APU-off and 1 for APU-on.

Dynamic programming (DP) is considered in this study in order to provide the global optimal strategy to control the APU operations [25, 26]. It decides on the optimal strategy $U_{opt} = \{u(1), \dots, u(N)\}_{opt}$

for the scheduled route at each instant t while minimizing the fuel cost function J presented in equation (11). Consequently, DP computes backward in time from the final desired battery state of charge SOC_f to the initial state SOC_i the optimal fuel mass flow rate $\dot{m}_f\big(SOC(t), u(t)\big)$ in the discretized state time space as per equations (12) to (14). The generic DP function presented in [35] is considered in this study, with the battery SOC as state variable $x(t)$ and the APU start operations as control variable $u(t)$.

Note that the resulting optimal APU on/off strategy U_{opt} must not cause the components to violate their relevant physical boundary constraints in terms of speed, power or SOC, in order to ensure their proper functioning within the normal operation range. These constraints are included in the DP model and summarized in equations (15) to (22). It is also noteworthy to mention that using DP as APU energy management strategy excludes the impact of rule-based energy management strategy currently used on hybrid vehicles on the consumption. Consequently, the obtained fuel consumption results with DP are only dependant on the investigated energy converter and its efficiency.

$$J = min\left\{\sum_{t=1}^{N} \dot{m}_f\big(SOC(t), u(t)\big) \times dt_s\right\} \tag{11}$$

with

discrete step time:	$dt_s = 1$	(12)
number of time instances:	$N = \frac{n}{dt_s}$ (with *n* the time length of the driving cycle)	(13)
state variable equation:	$SOC(t+1) = f\big(SOC(t), u(t)\big) + SOC(1)$	(14)
initial SOC:	$SOC(1) = SOC_i$	(15)
final SOC:	$SOC(N) = SOC_f$	(16)
SOC constraint:	$SOC(t) \in [0.2, 0.9]$	(17)
battery power constraint:	$P_{b_{min}} \leq P_b(t) \leq P_{b_{max}}$	(18)
motor torque constraint:	$P_{m_{min}}\big(\omega_m(t)\big) \leq P_m(t) \leq P_{m_{max}}\big(\omega_m(t)\big)$	(19)
motor speed constraint	$0 \leq \omega_m(t) \leq \omega_{m_{max}}(t)$	(20)
generator power constraint:	$P_{g_{min}}\big(\omega_m(t)\big) \leq P_g(t) \leq P_{g_{max}}\big(\omega_m(t)\big)$	(21)
generator speed constraint:	$0 \leq \omega_g(t) \leq \omega_{g_{max}}(t)$	(22)

4. Results and discussion

Two different SHEV configurations are compared in this section: the suggested IRRGT-APU and a reference ICE-APU. The IRRGT-APU is designed to operate at its optimal operating point and delivers 40 kW of mechanical power. The ICE-APU uses a 1.2 liters spark ignition engine with maximum efficiency of 37%. During APU operations, the ICE is allowed to operate at any point of its torque-speed map. For both models, gasoline is the fuel used, and the simulations are performed on a sequence of one to five-repeated WLTP driving cycles (23 km each), covering driving distances up to 115 km.

The potential of fuel savings of IRRGT-APU compared to the ICE-APU is carried out under two sets of simulations. The first set emulates the behavior of plug-in hybrids and extended-range electric vehicles (denoted xEV in this section), with the option of battery charging from the grid. Simulations are performed at an initial SOC of 80% and a final SOC by the end of the trip at 30%. APU operation and battery SOC results are illustrated in appendix B, figure B.1. The second set of simulations emulates the behavior of self-sustaining hybrids with a zero use of electric energy from the battery at

the end of the cycle. Hence, the initial and final battery SOCs are set at 60%. APU operation and battery SOC results are illustrated in figure B.2.

Figure 11(a) highlights the potential of increasing the battery capacity on reducing the fuel consumption for both IRRGT-APU and ICE-APU. It illustrates the battery electric consumption per driven kilometer as function of the observed fuel consumption on one to five-repeated WLTP driving cycles. Two conclusions are drawn out of this figure:

1. A trade-off between the fuel consumption and the electric consumption is made. Large battery capacities induce lower fuel consumption and more reliance on electric energy. The governing equation of this energy trade-off is expressed in equation (23), with d the driving cycle length, $E_{b_{traction}}$ the battery electric energy consumption to overcome the vehicle traction load, E_{ber} the vehicle load energy recovered through regenerative braking, E_{fuel} the energy of the consumed fuel and E_{grid} the consumed electric energy from the grid to recharge the battery from 30% to 80% SOC. Therefore, for a given driving cycle length d ($E_{b_{traction}}$ and E_{ber} remain constant), thus increasing the battery capacity induces higher charging energy from the grid (E_{grid}) and lower fuel consumption (E_{fuel}).

$$\frac{E_{b_{traction}}}{d} = \frac{1}{d}\left(E_{ber} \times \eta_m + E_{fuel} \times \eta_{APU} + E_{grid} \times \eta_{charging}\right) \quad (23)$$

2. Higher fuel consumption is observed in the ICE-APU SHEV model compared to IRRGT-APU, for the four battery capacities. Assuming the same driving cycle length d, and for a given battery capacity, $E_{b_{traction}}$, E_{ber} and E_{grid} are the same for both models; consequently, improving the APU efficiency induces a decrease in fuel consumption, as expressed in (23). Accordingly, the IRRGT-APU performs more efficiently than the ICE-APU, and the IRRGT SHEV vehicle shows longer electric drive range (with the APU off), which leads to a higher powertrain efficiency, as illustrated in figure 12(a). The powertrain efficiency is computed using equation (24). It is noteworthy to mention that for short driving cycle length d (1 WLTP) and large battery capacities (10 and 20 kWh), the APU is not required to turn on, and the whole distance is travelled in electric mode only. Thus, the electric consumption of both models converges to 210 Wh/km for the 10 kWh battery and 217 Wh/km for the 20 kWh, as illustrated in figure 12(a). The additional consumption of the 20 kWh battery is due to the additional carried weight of the battery.

$$\eta_{powertrain} = \frac{E_{traction\ load}}{E_{ber} + E_{fuel} + E_{grid}} \quad (24)$$

(a)

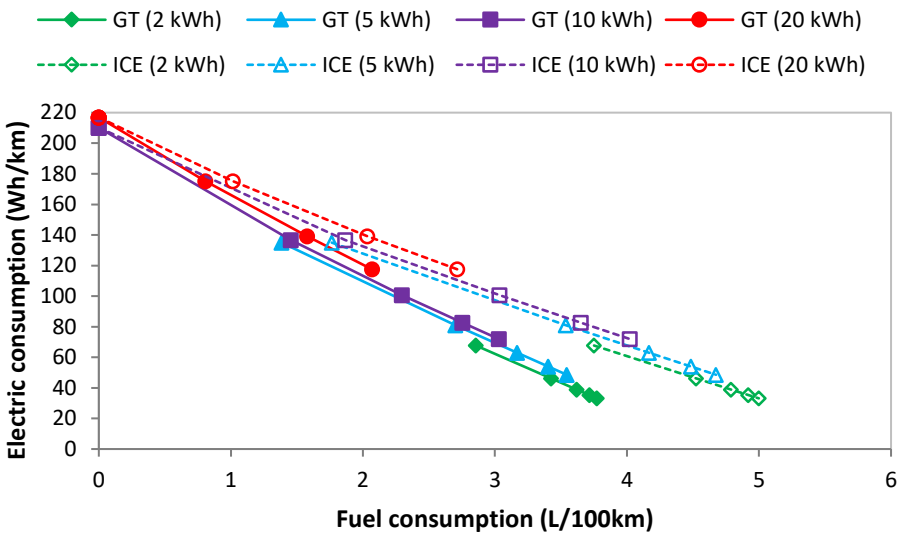

(b)

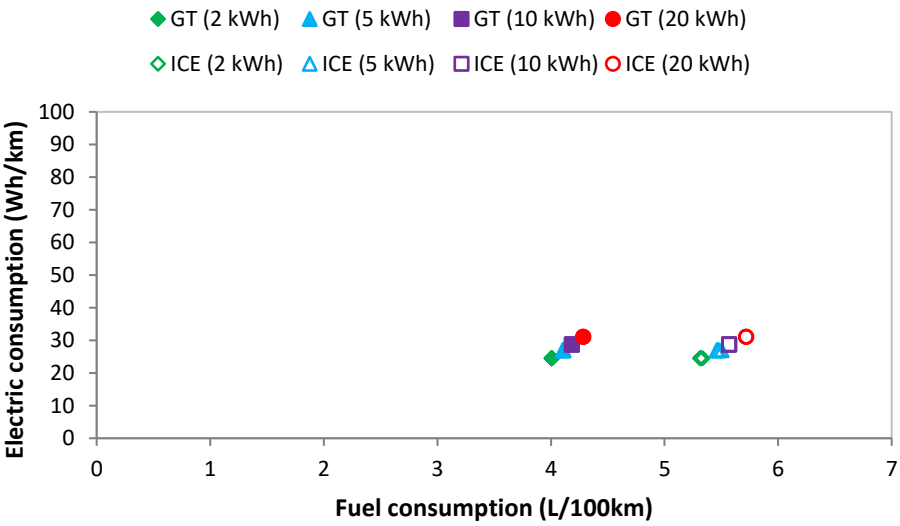

Fig. 11. Battery and fuel energy trade-off for (a) the xEV configuration and (b) the self-sustaining configuration, on one to five-repeated WLTP, under the four investigated battery capacities.

(a)

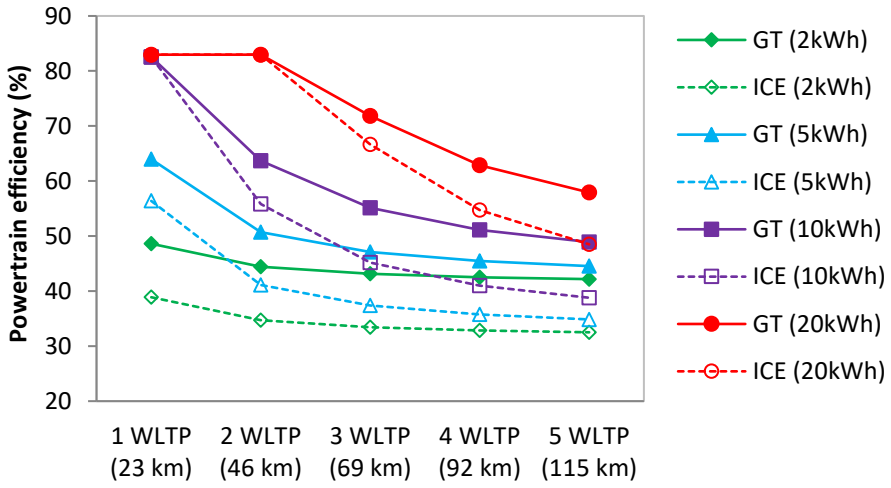

(b)

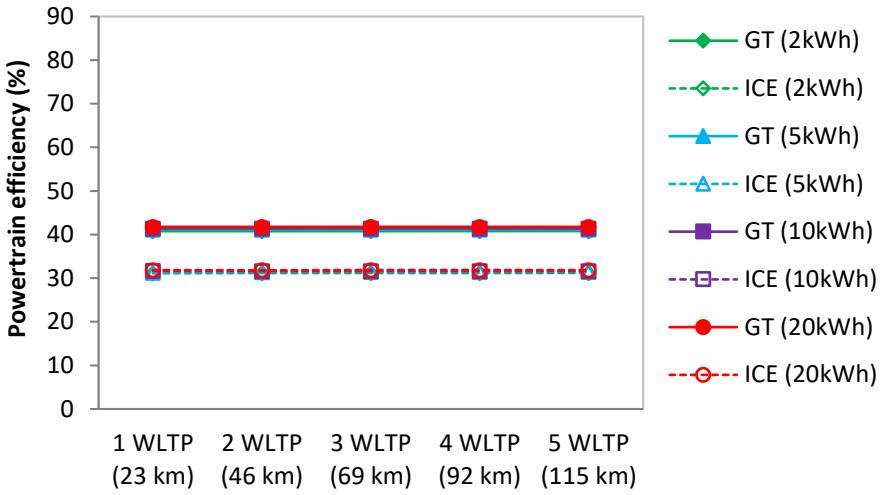

Fig. 12. Powertrain efficiency of (a) the xEV configuration and (b) the self-sustaining configuration, on one to five-repeated WLTP.

Figure 11(b) illustrates the battery electric consumption of the self-sustaining IRRGT-APU and ICE-APU models as function of the observed fuel consumption. According to the literature, the battery capacities in self-sustaining hybrids are relatively small (less than 3 kWh) when compared to xEVs, since batteries are used as energy buffers. This is confirmed in figure 11(b), where the electric energy consumed per driven kilometer are of the same magnitude for each of the two vehicle models, independently from the battery capacity. Hence, 7% more fuel is consumed with the 20 kWh battery when compared to the 2 kWh battery, as illustrated in figure 11(b). The additional consumption is explained by the unnecessary additional carried mass of the 20 kWh battery, serving only as energy buffer.

On the other hand, similarly to xEV configuration, the ICE-APU SHEV model shows higher fuel consumption compared IRRGT-APU, for the four battery capacities. This is explained in equation (25), where for the same driving cycle length d, and for a given battery capacity, $E_{b_{traction}}$ and E_{ber} are the same for both models; consequently, improving the APU efficiency induces a decrease in fuel consumption. This also leads to a higher powertrain efficiency of the IRRGT-APU SHEV, as illustrated in figure 12(b).

$$\frac{E_{b_{traction}}}{d} = \frac{1}{d}\left(E_{ber} \times \eta_m + E_{fuel} \times \eta_{APU}\right) \tag{25}$$

Comparing between figures 12(a) and (b), it is noteworthy to mention that the powertrain efficiency of the xEV configuration converges toward the efficiency of the self-sustaining model as the driving cycle length d exceeds 100 kilometers. In fact, when d tends to infinity, the battery energy consumption ($E_{b_{traction}}$) to overcome the traction load in xEV configuration expressed in equation (23) could be simplified by eliminating the term (E_{grid}/d), and therefore, $E_{b_{traction}}$ tends to the battery consumption of the self-sustaining configuration expressed in equation (25).

(a)

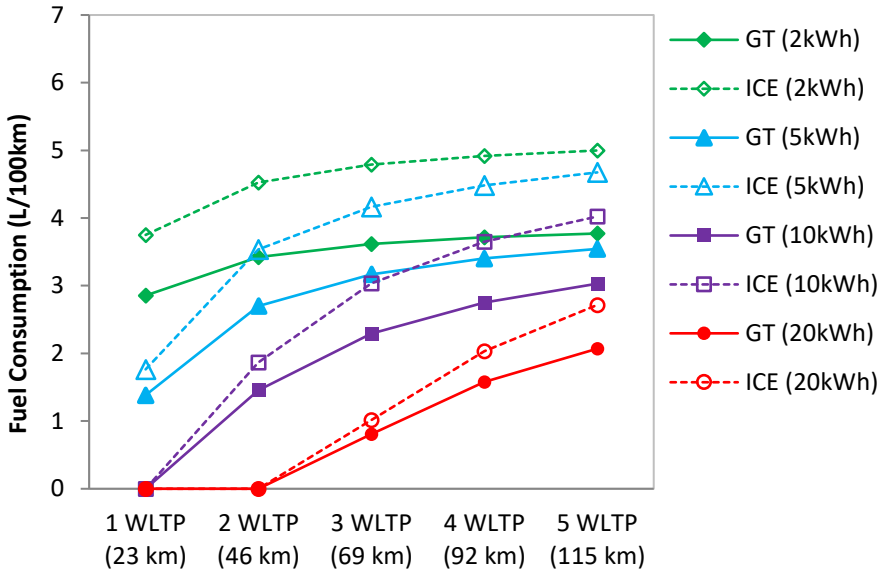

(b)

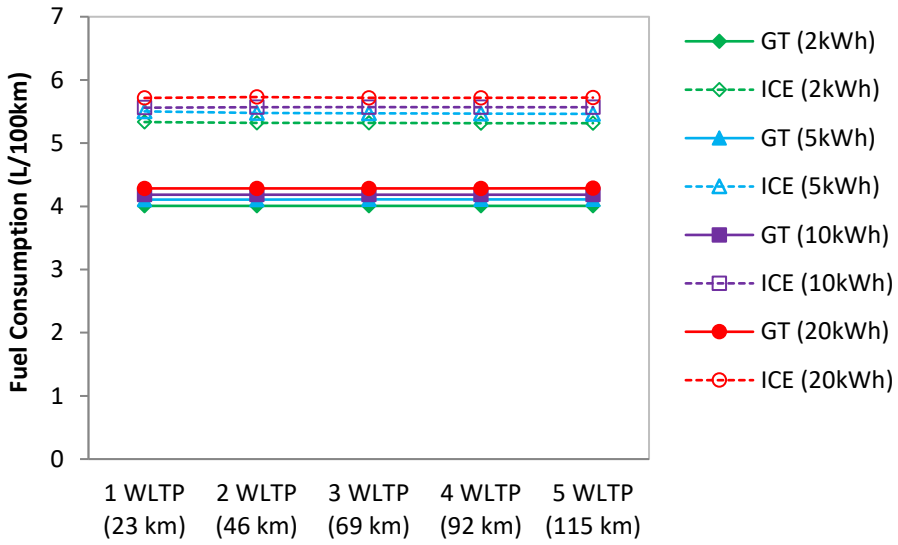

Fig. 13. Fuel consumption results between IRRGT-system and ICE of (a) the xEV configuration and (b) the self-sustaining configuration, on one to five-repeated WLTP.

Finally, comparing the fuel consumption results between the IRRGT-APU and the ICE-APU (figures 13(a) and 13 (b)), 22% to 25% fuel savings are observed under the two sets of simulations, the self-sustaining and the xEV configurations. As detailed above, these savings are explained by the higher operating efficiency of the IRRGT since it was constrained to operate at its optimal efficiency of 47%. Although the ICE was not constrained to operate at one operating point, results showed that ICE operation was at the optimal operating line (OOL) where the efficiency remains between 36 and 37%, almost at its maximum efficiency of 37%.

5. Conclusion and perspectives

An exergo-technological explicit method considering energy and exergy analysis, as well as components and automotive technological constraints was applied in this study to identify the suitable GT-system for series hybrid vehicle applications. The Intercooled Regenerative Reheat Gas Turbine (IRRGT) was selected. It offered the best combination of high efficiency and power density compared

to the investigated realistic GT-systems and to conventional internal combustion engines. A series hybrid vehicle was modeled and the IRRGT-APU and ICE-APU energy converters are simulated and compared in term of fuel consumption using the DP optimal control as APU management strategy. A parametric study was also conducted in order to evaluate the impact of battery capacity and mass on fuel consumption.

Simulation results showed that the IRRGT-system series hybrid configuration offers 22% to 25% fuel consumption savings compared to similar ICE configuration. Results also highlighted the interest of considering large battery capacities for maximizing fuel savings in series hybrids under xEV configuration. 61% of fuel savings were observed between extended-range IRRGT-APU series vehicle with 20 kWh battery and a self-sustaining ICE-APU series hybrid with a 2 kWh battery capacity. However, this advantage came at the expense of an increased vehicle cost and battery volume, which was not discussed in this study.

In addition to the fuel savings, the IRRGT-system offered other intrinsic automotive advantages such as reduced mass compared to ICE, suitable vehicle integration as well as multi-fuel use capability, which makes it a potential energy converter option for implementation on series hybrid powertrains in the future.

The methodology presented in this study will be further elaborated in order to evaluate the fuel consumption saving for GT-systems on different vehicle applications ranging from small to large and SUV vehicles. Simulations will include Real Driving Cycles (RDE) and other vehicle energy criteria such as the cabin thermal needs. Moreover, the selected IRRGT cycle will be further investigated with water injection at different locations in the machine such as downstream the second compressor in order to maximize heat recovery through the regenerator as well as to reduce pollutant emissions, mainly nitrogen oxide.

References

[1] History of Chrysler Corporation Gas Turbine Vehicles, Chrysler Corporation, January 1979.

[2] Huebner G Jr. The Chrysler regenerative turbine-powered passenger car. Society of Automotive Engineers, In: *Automotive Engineering Congress and Exposition*, Detroit, January 13-17, 1964.

[3] Cunha H. Investigation of the Potential of Gas Turbines for Vehicular Applications. Chalmers University of Technology, Gothenburg, Sweden, Master's thesis 2011.

[4] Capata R, Coccia A and Lora M. A Poposal for CO2 abatement in urban areas: the UDR1 - Lethe Turbo-Hybrid Vehicle. University of Roma 1 “La Sapienza”, Italy, *Energies* ISSN 1996-1073.

[5] Davidson J and Keeley R. The thermodynamics of practical combined cycles. In: *Proc. Instn. Mech. Engrs*. Conference on Combined Cycle Gas Turbines, 28-50, 1991.

[6] Briesch S, Bannister L, Dinkunchak S. and Huber J. A combined cycle designed to achieve greater than 60% efficiency. ASME J. Eng Gas Turbines Power 117(1), 734-741, 1995.

[7] Nada T. Performance Characterization of different configurations of gas turbine engines. Propulsion and Power Research, September 2014.

[8] Patil M, Pawase D and Deore E. Thermal performance of reheat regenerative intercooled gas turbine cycle. IJRMET Vol. 5, May-October 2015.

[9] Bhargava R, Bianchi M, De Pascale A et al. Gas turbine based power cycles – A state-of-the-art review. In: *International Conference on Power Engineering*. Hangzhou, China, 2007.

[10] Dellenback P. Improved gas turbine efficiency through alternative regenerator configuration. In: *J. of Eng. for Gas Turbines and Power*, Vol. 124, pp 441-446, 2002.

[11] Pathiranthna K. Gas turbine thermodynamic and performance analysis methods using available catalog data. University of Gävle, Faculty of engineering and sustainable development, October 2013.

[12] El-Masri M. A modified high efficiency recuperated gas turbine cycle. In: *Journal of Eng for Gas Turbines and Power*. Vol. 110, pp 233-242, 1988.

[13] El-Masri M. Thermodynamics and performance projections for intercooled / reheat / recuperated gas turbine systems. ASME Paper No. 87-GT-108, 1987.

[14] Cheng D and Nelson A. The chronological development of the Cheng cycle steam injected gas turbine during the past 25 years. ASME Paper No. GT-2002-30119, 2002.

[15] Kulshreshtha D and Mehta S. Exergy Analysis of a Regenerative Micro Gas Turbine Engine. In: *Proceedings of ICFD 10: Tenth International Congress of Fluid Dynamics*. December 16-19, 2010.

[16] Sirignano W and Liu F. Performance increase for gas-turbine engines through combustion inside the turbine. In: *Journal of Propulsion and Power*. Vol.15, No. 1, January - February 1999.

[17] Andriani R, Gamma F and Ghezzi U. Main effects of intercooling and regeneration on aeronautical gas turbine engines. In: *46th AIAA/ASME/SAE/ASEE Joint Propulsion Conference & Exhibit.* Nashville, TN, 25 - 28 July 2010.

[18] Christodoulou F, Giannakakis P and Kalfas A. Performance benefits of a portable hybrid micro-gas-turbine power system for automotive applications. In: *Proceedings of ASME Turbo Expo 2010: Power for Land, Sea, and Air*. GT2010-23248, 2010.

[19] Capata R, Sciubba E and Toro C. The gas turbine hybrid vehicle LETHE at UDR1: The on-board innovative ORC energy recovery system – feasibility analysis. In: *Proceedings of the International Mechanical Engineering Conference & Exposition*, Houston, Texas, 2012.

[20] Shah B, Mazuir R, McGordon et al. Micro gas turbine range extender – validation techniques for automotive applications. In: *4th Hybrid Electric Vehicle Conference*, London, United Kingdom, 2013.

[21] Mackay R. Development of a 24 kW gas turbine-driven generator set for hybrid vehicles. In: *International congress and exposition*, Detroit, Michigan, SAE technical paper series, 940510, 1994.

[22] Leontopoulos C, Etemad M, Pullen R and Lamperth M. Hybrid Vehicle simulation for a turbogenerator based power-train. *Proceedings of the Institution of Mechanical Engineers*. Part D: *Journal of Automobile Engineering*, Vol 212, pp 357-368, 1998.

[23] Lampérth U, Pullen K and Mueller K. Turbogenerator based hybrid versus dieselelectric hybrid-A parametric optimization simulation study. In: *2000 Future Transportation Technology Conference*, Costa Mesa, California, SAE Paper No. 2000-01-3100, 2000.

[24] Juhasz A. Automotive gas turbine power system - Performance analysis code. *In: the 1997 International Congress and Exposition.* Lewis Research Center, NASA Technical Memorandum 107386, 1997.

[25] Mansour C. Trip-based optimization methodology for a rule-based energy management strategy using a global optimization routine: the case of the Prius plug-in hybrid electric vehicle. In: *Proceedings of the Institution of Mechanical Engineers*. Part D: *Journal of Automobile Engineering*, Vol 230, Issue 11, pp. 1529 – 1545, 2015.

[26] Mansour C. Optimized energy management control for the Toyota Hybrid system using dynamic programming on a predicted route with short computation time. *In: International Journal of Automotive Technology.* Paper N° 220100321, vol.13, No. 2, 2012.

[27] Sonntag R and Borgnakke R. Fundamentals of Thermodynamics, Sixth Edition, 2003, p.411-423.

[28] Moran M and Shapiro H. Fundamentals of engineering thermodynamics. 5th Edition – 2006, p.303-308.

[29] Hadid Z and Zoughaib A. Exergy recovery during LNG gasification using ambient air as heat source, In: *Proceedings of Ecos 2016 – The 29th international conference on efficiency, cost, optimization, simulation and environmental impact of energy systems.* Portoroz, Slovenia, June 19-23, 2016.

[30] Dev N and Attri R. Exergetic analysis of a combustion chamber of a combined heat and power system. In: *Proceedings of the National Conference on Trends and Advances in Mechanical Engineering.* YMCA University of Science & Technology, Faridabad, Haryana, Oct 19-20, 2012.

[31] Datta A and Som S. Energy and exergy balance in a gas turbine combustor. J Power Energy - Proc Inst Mech Eng, 213:23–32, 1999.

[32] Jubleh N. Exergy analysis and second law efficiency of a regenerative brayton cycle with isothermal Heat Addition. Entropy ISSN 1099-4300, 2005.

[33] Linnemann C and CONEY M. The isoengine: realization of a high efficiency power cycle based on isothermal compression. In: *International Journal of Energy Technology and Policy*, Vol. 3, 2005.

[34] Deb K, Pratap A, Agarwal S et al. A fast and elitist multiobjective Genetic Algorithm: NSGA-II. In: *IEEE Transactions on evolutionary computation*, Vol. 6, No. 2, APRIL 2002.

[35] Sundstrom O and Guzzella L. A generic dynamic programming Matlab function. *2009 IEEE Control Applications, (CCA) & Intelligent Control, (ISIC)*. St. Petersburg, 2009, pp. 1625-1630. doi: 10.1109/CCA.2009.5281131

[36] Mehrdad E, Yimin G and Ali E. Modern Electric, Hybrid electric, and Fuel Cell Vehicles, Fundamentals, Theory, and Design, Second Edition, p.254.

Appendix A

SHEV powertrain components sizing

This appendix presents the equations used for the SHEV powertrain components sizing. Demonstration can be further consulted in [37]. Equation (A.1) computes $P_{m_{acc}}$, the tractive power required to accelerate the vehicle from zero to V_f in t_a seconds. Note that V_b the vehicle velocity corresponding to the motor base speed.

$$P_{m_{acc}} = \frac{M_t}{2t_a}\left(V_f^2 + V_b^2\right) + \frac{2}{3}M_t g f_r V_f + \frac{1}{5}\rho C_x S V_f^3 \tag{A.1}$$

Equation (A.2) presents the GT-system average power required to maintain the battery energy sufficiently sustained under stop-and-go urban-driving patterns. Note that t_c corresponds to the driving cycle time length.

$$P_{GT} = \frac{1}{\eta_g}\left(\frac{1}{t_c}\int_0^{t_c}\left(M_t g f_r + \frac{1}{2}\rho_a C_x S V^2\right)V dt + \frac{1}{t_c}\int_0^{t_c} M_t \frac{dV}{dt} dt\right) \tag{A.2}$$

Equation (A.3) computes the continuous power required from the GT-system in order to maintain the vehicle cruising for long distance at a certain speed V on highway without the support of the battery.

$$P_{GT} = \frac{1}{\eta_g}\left(\frac{V}{\eta_t \eta_m}.(M_t g f_r + \frac{1}{2}\rho_a C_x S V^2)\right) \quad \text{(A.3)}$$

Equation (A.4) determines the minimum battery power required to propel the vehicle under any driving patterns.

$$P_b \geq \frac{P_{m_{max}}}{\eta_m} - P_{GT}\eta_g \quad \text{(A.4)}$$

Appendix B

xEV and self-sustaining SHEV simulation results

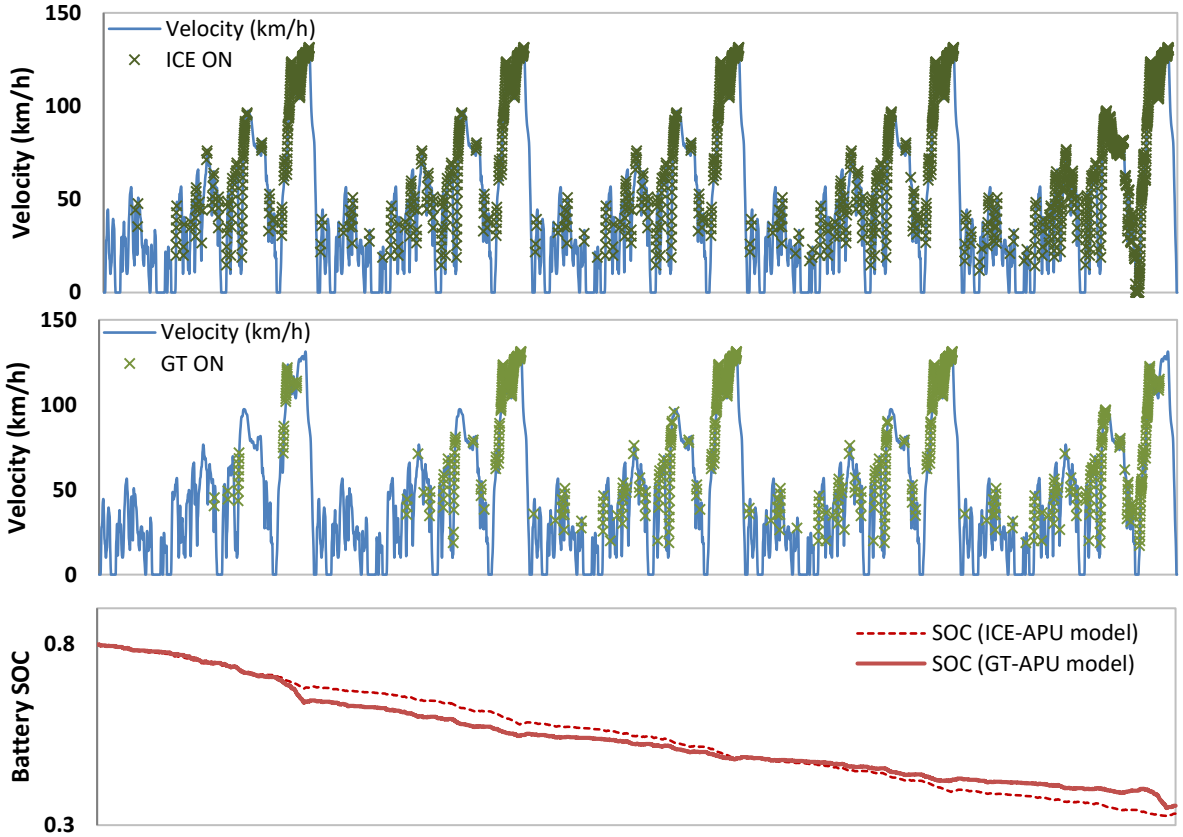

Fig. B.1. Results emulating SHEV with 20 kWh battery on 5 WLTP (SOCi = 80%, SOC_f = 30%).

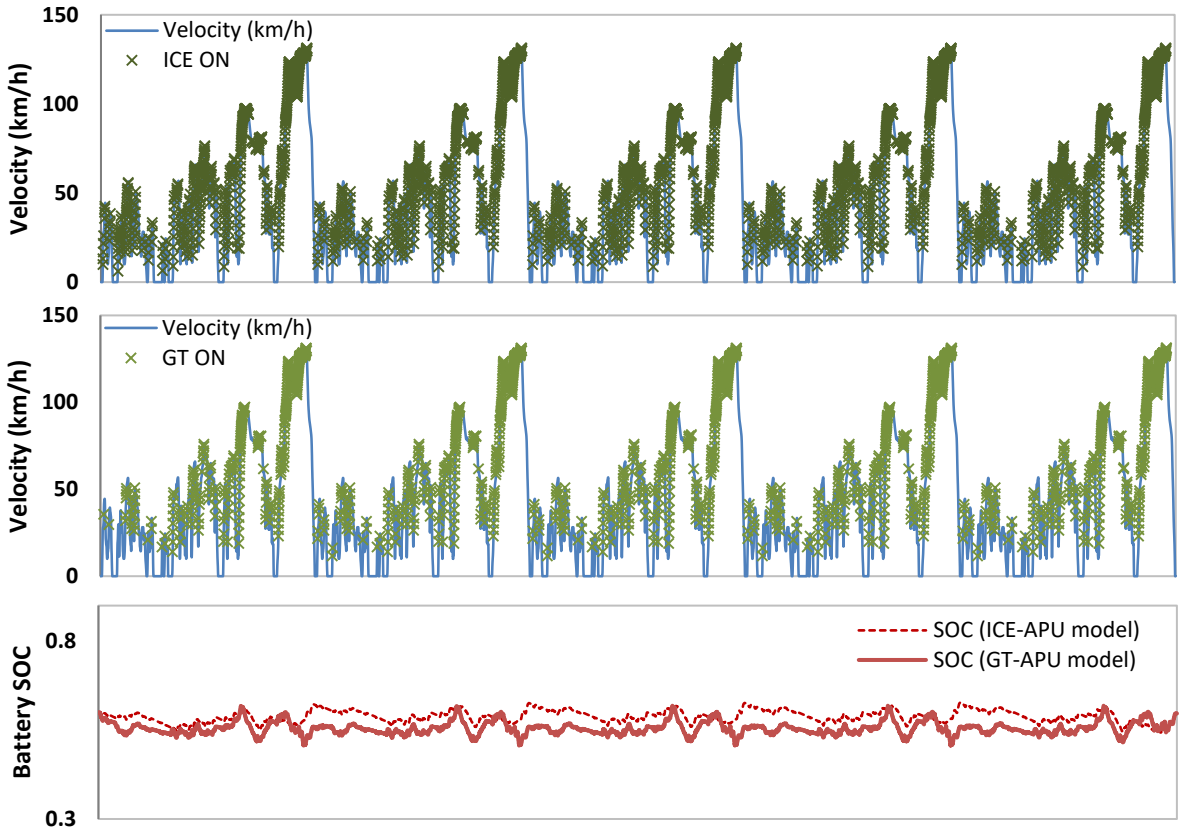

Fig. B.2. Results emulating SHEV with 2 kWh battery on 5 WLTP ($SOCi = SOC_f = 60\%$).